RESEARCH ARTICLE

Key Points:
- Trace elements co-vary with marine productivity proxies during warm climates
- Productivity controls pore water oxygen and sedimentary redox conditions
- Cordilleran ice sheet directly affected productivity and sedimentary redox

Supporting Information:
- Readme
- Table S1

Correspondence to:
A. S. Chang,
alice.chang@ubc.ca

Effects of productivity, glaciation, and ventilation on late Quaternary sedimentary redox and trace element accumulation on the Vancouver Island margin, western Canada

Alice S. Chang[1], Thomas F. Pedersen[1], and Ingrid L. Hendy[2]

[1]School of Earth and Ocean Sciences, University of Victoria, Victoria, British Columbia, Canada, [2]Department of Earth and Environmental Sciences, University of Michigan, Ann Arbor, Michigan, USA

Abstract Variations in chalcophile and redox-sensitive trace elements are examined at high-resolution intervals from a ~50 kyr long sediment core (MD02-2496) from the Vancouver Island margin. Enrichments of Ag, Cd, Re, U, and Mo above lithogenous levels, signifying sedimentary suboxia and anoxia, occurred during the early Holocene and Bølling/Allerød, and during warm interstadial events of Marine Isotope Stage (MIS) 3. Down-core trace element profiles co-vary with productivity proxy records (opal, $CaCO_3$, and marine organic carbon), and with sedimentary nitrogen isotope ratios, which reflect variably enriched nitrate upwelled from intermediate waters that were transported northward from the Eastern Tropical North Pacific. The similarity of the MD02-2496 record with records from the southern portion of the California Current System (CCS), and to the Greenland ice core oxygen isotope record during warm climate intervals, suggests that sedimentary redox conditions along the California Current responded to local productivity, to North Atlantic climate change and to tropical Pacific surface water processes via long-distance teleconnections. Concentrations of trace elements and productivity proxies were relatively depleted during the Younger Dryas, cool stadial events of MIS 3, and in two episodes of glaciomarine sedimentation from ~14.7 to 30.5 kyr BP (last glacial maximum, LGM), and from 44 to 50.4 kyr BP. Cordilleran Ice Sheet advancement onto the Vancouver Island continental shelf during the LGM led to intervals of increased terrigenous sedimentation and greatly reduced productivity not seen in the southern portion of the CCS, and along with ventilation of North Pacific Intermediate Waters, resulted in brief sedimentary oxic conditions.

1. Introduction

Using a suite of chalcophile and redox-sensitive trace elements for determining sedimentary paleoredox conditions in continental margin settings has become an established method [e.g., *Morford and Emerson*, 1999; *Böning et al.*, 2004; *Sundby et al.*, 2004; *Cartapanis et al.*, 2011]. Bottom and pore water oxygen contents are assumed to change as a result of fluctuations in ocean ventilation and/or primary productivity that affect the oxygen minimum zone (OMZ). Along the California Current System (CCS), the OMZ is influenced by a balance between the nutrient-rich but oxygen-poor Subtropical Subsurface Water (SSW) advected northward by the California Undercurrent from the Eastern Tropical North Pacific (ETNP) [*Hickey*, 1979; *Thomson and Krassovski*, 2010], and by well-oxygenated North Pacific Intermediate Water (NPIW) ventilated from the Sea of Okhotsk, the Bering Sea, and the Gulf of Alaska [*Talley*, 1991; *Van Scoy et al.*, 1991; *Takahashi*, 1998]. High primary and export production resulting from enhanced coastal upwelling lead to increased oxygen consumption as settling organic matter decays through the water column and on the seafloor [*Wyrtki*, 1962]. Because trace elements each have different redox behaviors, a combination of different trace element enrichments can help constrain whether the sedimentary pore waters were oxic, suboxic (no dissolved oxygen but trace sulfides present), or anoxic (no oxygen, measurable sulfides present) at the time of deposition. Using trace elements in conjunction with paleoproductivity proxies such as organic carbon (C_{org}), $CaCO_3$, biogenous Ba (barite), or biogenous silica (opal) can further illustrate how trace element accumulation in the sediments is influenced by productivity [e.g., *Algeo and Lyons*, 2006; *McKay and Pedersen*, 2008; *Wagner et al.*, 2013].

Numerous studies involving records spanning at least the last 50 kyr from the southern expanse of the CCS have used trace elements and productivity proxies to decipher productivity and oxygenation histories on glacial to interglacial time scales [e.g., *Dean et al.*, 2006; *Nameroff et al.*, 2004; *Cartapanis et al.*, 2011].
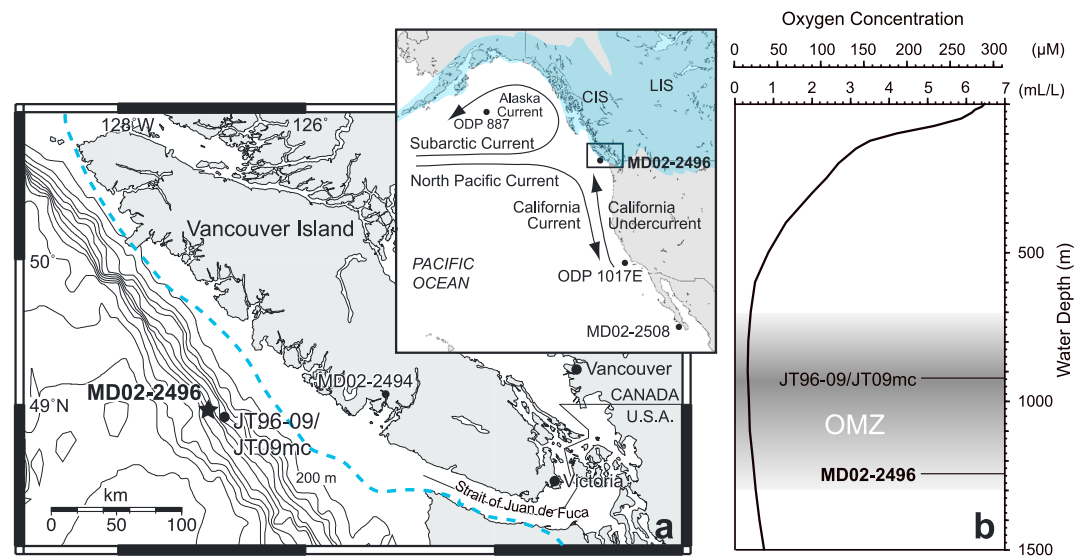
Figure 1. Study area, ocean properties, and ice sheet extent. (a) Ocean currents and location of cores discussed in this study. Bathymetric contour intervals at 200 m. Dashed blue line shows the approximate extent of ice at the last glacial maximum (LGM) [*Clague and James*, 2002]. Blue shaded area in inset is the approximate continental ice coverage during the LGM, redrawn from *Andersen and Borns* [1997]. CIS: Cordilleran Ice Sheet. LIS: Laurentide Ice Sheet. (b) Oxygen concentration profile from coordinates 48.5°N, 126.5°W [*Garcia et al.*, 2006], with core depths highlighted. Shaded area represents the depth of the oxygen minimum zone (OMZ).

Comparisons between trace element records with stable nitrogen isotope ratios (δ^{15}N) have also been made [*Ivanochko and Pedersen*, 2004; *Hendy and Pedersen*, 2005] and show how relative nutrient utilization [*Altabet and François*, 1994] and denitrification [*Ganeshram and Pedersen*, 1998] in the ETNP and the export of oxygen-poor water masses have changed over time [*Kienast et al.*, 2002].

Despite such extensive research, a sediment record of similar duration at the northernmost extent of the CCS is lacking. In this study, core MD02-2496 (Figure 1a), raised in 2002 during the International Marine Global Changes-Marges Ouest Nord Américaines (IMAGES-MONA) program [*Beaufort et al.*, 2002], extends the Vancouver Island margin sediment record to 50 kyr, complementing the nearby 16 kyr long core (JT96-09) obtained by *McKay et al.* [2004, 2005]. New high-resolution major, minor, and trace element data from MD02-2496 are compared with previously published sedimentology [*Cosma and Hendy*, 2008; *Cosma et al.*, 2008], and δ^{15}N, productivity proxy, and Mo data [*Chang et al.*, 2008], in order to refine the sedimentary redox history of a region that was in close proximity to an ice sheet during the last glacial maximum (LGM)—a dynamic that was not encountered in the southern locations.

The waters off the west coast of Canada are influenced by the bifurcation of the eastward flowing Subarctic and North Pacific currents into the northward flowing Alaska Current and the southward flowing California Current as a result of a divergence in prevailing wind directions (Figure 1a). Although the source mechanism is not completely understood, subsurface pressure gradients cause the California Undercurrent to flow poleward along the western North American margin [*Hickey*, 1979; *Thomson and Krassovski*, 2010]. The undercurrent flows at a depth of 125–325 m off southwestern Vancouver Island, with core speeds at depths between 200 and 275 m [*Reed and Halpern*, 1976; *Huyer et al.*, 1998; *Pierce et al.*, 2000]. A combination of seasonal, wind-driven upwelling of nutrients drawn from the SSW, local bottom topography, and estuarine-driven mixing and outflow from the Juan de Fuca Strait [*Thomson et al.*, 2007; *Allen and Hickey*, 2010] leads to sustained primary productivity reaching up to 425 g C/m^2/yr off southwestern Vancouver Island [*Antoine et al.*, 1996]. From sediment trap studies in the region, diatoms are assumed to be the major phytoplankton group, with other groups such as coccolithophores being lesser contributors [*Peña et al.*, 1999; *Chang et al.*, 2013]. A distinct OMZ currently lies between depths of 700 and 1300 m, but it is most pronounced at ~920 m depth where oxygen concentrations are between 14 and 22 μM (Figure 1b) [*McKay et al.*, 2005; *Garcia et al.*, 2006]. The oceanography and sedimentology of the Vancouver Island margin region were impacted by the Cordilleran Ice Sheet (CIS) during the last (Fraser) glaciation (~30.5–14.7 kyr BP), as ice filled coastal waterways

Table 1. Recommended and Measured Values for Standard Reference Materials

MESS-3 (Marine Sediment)[a]	Ag (ng/g)	Cd (μg/g)	Re (ng/g)	Mo (μg/g)	
Recommended	180 ± 20	0.24 ± 0.01	n.d.[b]	2.78 ± 0.07	
Measured	186 ± 20	0.23 ± 0.02	3.49 ± 0.31	2.91 ± 0.34	
% RSD[c]	11	6.97	8.98	11.55	
n	130	123	121	109	
SY-4 (diorite gneiss)[a]	Al_2O_3 (wt. %)	Fe_2O_3 (wt. %)	MnO (wt. %)	Ba (μg/g)	U (μg/g)
Recommended	20.69 ± 0.08	6.21 ± 0.03	0.108 ± 0.001	340 ± 5	0.8 ± 0.1
Measured	20.40 ± 0.32	6.24 ± 0.04	0.106 ± 0.008	339 ± 24	0.8 ± 0.1
% RSD[c]	1.58	0.69	7.443	7	10.1
n	7	7	7	7	7
JB-2 (basalt)[d]	Al_2O_3 (wt. %)	Fe_2O_3 (wt. %)	MnO (wt. %)	Ba (μg/g)	U (μg/g)
Recommended	14.64 ± 0.27	13.31 ± 0.41	0.218 ± 0.013	222 ± 31	0.180 ± 0.067
Measured	14.43 ± 0.47	14.21 ± 0.55	0.214 ± 0.007	223 ± 9	0.163 ± 0.017
% RSD[c]	3.27	3.86	3.087	4	10.578
n	33	33	33	33	33

[a]National Research Council of Canada.
[b]n.d.: not determined.
[c]Relative standard deviation.
[d]Geological Survey of Japan.

and delivered lithogenous sediment to the shelf. The CIS approached within 35 km of the MD02-2496 coring site at ~20 kyr BP (Figure 1a) [*Clague et al.*, 1980; *Herzer and Bornhold*, 1982; *Cosma et al.*, 2008]. Thus, the sedimentary geochemistry in this area is a highly sensitive archive of both climatic and oceanographic changes.

2. Methods

The 38.35 m long, 10 cm diameter MD02-2496 Calypso core was recovered by the R/V *Marion Dufresne* at 48° 58.47′ N and 127°02.14′ W from a water depth of 1243 m, near the lower boundary of the present-day OMZ. An age model for MD02-2496 was constructed using 36 AMS ^{14}C measurements of mixed planktonic foraminifera, one measurement of mixed benthic foraminifera, and seven measurements of bulk sediments in the upper section of the core that lacked foraminifera. Age model calibrations and calculated calendar years and errors are described in *Cosma et al.* [2008]. The top of the core is estimated to be at ~2300 yr BP, an offset that is commonly found for large-diameter piston corers, which typically fail to capture the uppermost sediment column. Climatic events older than ~40 kyr BP should be interpreted with caution because of the limitations of the radiocarbon method for ages greater than seven half-lives of ^{14}C and the associated large errors (±1–3.5 kyr) [*Cosma et al.*, 2008].

High-resolution geochemical analyses involved 759 samples taken at 4–5 cm intervals (uncorrected core depth), which represent ~10–125 years per interval, depending on the sedimentation rate. Samples at the start of the Holocene were collected at 2.5 cm intervals. The isotope dilution method was used for the analyses of trace Ag, Cd, Re, and Mo where 10–15 mg of freeze-dried and powdered sediment were mixed with weighed amounts of isotopically enriched and calibrated ^{109}Ag:^{107}Ag, ^{111}Cd:^{113}Cd, ^{185}Re:^{187}Re, and ^{95}Mo:^{98}Mo spike solutions (~1000 ppm, High-Purity Standards). Spiked samples, blanks, and a certified marine sediment standard (MESS-3; National Research Council of Canada) were digested in concentrated environmental grade HCl and HNO$_3$ and ultrapure grade HF acids inside closed Teflon vials using a Questron QLab 6000 microwave oven. The solutions were evaporated to dryness on a hotplate, and redissolved in 0.5N HCl in the oven. Recalcitrant organic residues were dissolved with H$_2$O$_2$ (30%, A.C.S. grade) on a hotplate. After a 100 μL aliquot of the final solution was removed for Mo analysis, the remaining solutions were passed through 10 mL polypropylene anion exchange columns containing 1 mL of acid-conditioned Dowex 1-X8 (100–200 mesh) chloride-form resin to pre-concentrate Ag, Cd, and Re and to remove polyatomic oxide interferences (^{91}Zr, ^{93}Nb, and ^{95}Mo). The final eluent was then evaporated to near-dryness. The Mo and Ag-Cd-Re solutions were each diluted in 1.25 mL of 1% HNO$_3$ and were analyzed separately with a Thermo X7 X-Series II quadrupole inductively coupled plasma mass spectrometer (ICP-MS) in peak jumping mode at the University of Victoria. Measured values for MESS-3 show acceptable analytical accuracy and precision with our methodology (Table 1).

The analyses of Al, Fe, Mn, Ba, and U were performed by ALS Geochemistry (North Vancouver, Canada) with a Varian inductively coupled plasma optical emission spectrometer for major elements and a Perkin-Elmer Elan 9000 ICP-MS for minor and trace elements. Two-hundred milligrams of freeze-dried and powdered sediment was fused with 900 mg of $LiBO_2$ at 1000°C, and the resulting glass dissolved in 10% HNO_3. Quality assurance was provided by analyzing the international rock standards JB-2 (basalt, Geological Survey of Japan) and SY-4 (diorite gneiss, National Research Council of Canada) prepared by the same method (Table 1).

Analytical details for the determination of sedimentary $\delta^{15}N$ ratios and $CaCO_3$, marine C_{org}, and opal concentrations are discussed in *Chang et al.* [2008]. Briefly, $\delta^{15}N$ was determined by continuous-flow isotope ratio mass spectrometry on chemically untreated sediments. Carbonate (inorganic) carbon was determined by acid evolution of CO_2 and coulometry, and total C_{org} was calculated as the difference between total carbon, measured by an elemental analyzer, and inorganic carbon. Due to input of terrigenous organic matter at MD02-2496, marine C_{org} is presented as the difference between the total and terrigenous C_{org} concentrations, the latter calculated using a mixing model [*Prahl et al.*, 1994] involving an assumed marine carbon isotopic end member value of −21‰ (VPDB) [*McKay*, 2003] and a terrigenous end member value of −27‰ [*McKay et al.*, 2004]. Opal was analyzed by alkaline dissolution-spectrophotometry [*Mortlock and Froelich*, 1989] at lower sampling intervals of 16–20 cm in the core, with some samples taken at 4–5 cm intervals. Analyses were repeated several times due to poor reproducibility, a common problem when opal contents are <10 wt. %. The $CaCO_3$, marine C_{org}, opal, and Mo concentrations from *Chang et al.* [2008] are updated, reflecting corrected salt-content calculations that affected mainly the top portion of the core (mid to late Holocene, <7% discrepancy). Salt determination was by Knudsen titration of the chloride content of distilled-water leaches of selected weighed sediment subsamples [*Strickland and Parsons*, 1968]. All concentration data are presented on a salt-free basis (Supplemental Table S1).

3. Results

3.1. Sediment Description

Core MD02-2496 consists of intervals of homogeneous olive gray silty clays, dark gray silty clays, and cyclical fining upward sequences of graded fine sands to silty clay in which bioturbation was common [*Beaufort et al.*, 2002] (Figure 2). Black opaque balls resembling pyrite were observed adhering to the surface of foraminifera tests (*M. Taylor and I. Hendy*, pers. obs. 2013). The olive gray silty clays correspond with color reflectance (*b**) in the yellow spectrum (organic rich), lower magnetic susceptibility (few magnetic minerals), and finer grain size, while the dark gray silty clays have reflectance in the blue spectrum (mineral rich), have higher magnetic susceptibility, and are coarser grained [*Cosma and Hendy*, 2008]. Peak deposition of coarse, glaciomarine ice-rafted debris (IRD) and dropstones occur during three intervals at ~46.5, ~16, and 14.7 kyr BP [*Cosma et al.*, 2008; *Hendy and Cosma*, 2008]. Sedimentation rates range from ~26 to 462 cm/kyr, with the highest rates occurring when the CIS was retreating but maintained a marine margin during the LGM (Figure 2).

3.2. Nitrogen Isotopes and Productivity Proxies

Relatively enriched $\delta^{15}N$ ratios and higher concentrations of $CaCO_3$ and marine C_{org} occur in hemipelagic sediments, and during the early Holocene, the Bølling/Allerød (B/A), and warm interstadials (IS) of Dansgaard-Oeschger (D-O) oscillations identified in the Greenland Ice Sheet Project 2 (GISP 2) record [*Dansgaard et al.*, 1993] (Figure 2). Depleted $\delta^{15}N$ ratios and lower productivity proxy concentrations occur during the YD, LGM, and cooler stadials, and in glaciomarine sediments older than ~44 kyr BP (Figure 2). Opal data do not have sufficient resolution to show D-O oscillations but generally co-vary with marine C_{org}. The Ba/Al profile is similar to marine C_{org} and opal after ~14.7 kyr BP but shows no correlation with D-O oscillations in the rest of the record.

3.3. Elemental Data

Total element concentrations, as well as metal/Al ratios, are presented in Figures 3 and 4, where the metal/Al ratios highlight the true metal variability in the absence of dilution by terrigenous or biogenous phases. Down-core variability between the concentration and metal/Al profiles is similar for each metal, suggesting that dilution effects are mostly minor.

Silver, Cd, Re, and Mo all show low metal/Al ratios near lithogenous background levels in glaciomarine sediments and during cool climatic intervals, and higher ratios in hemipelagic sediments and during
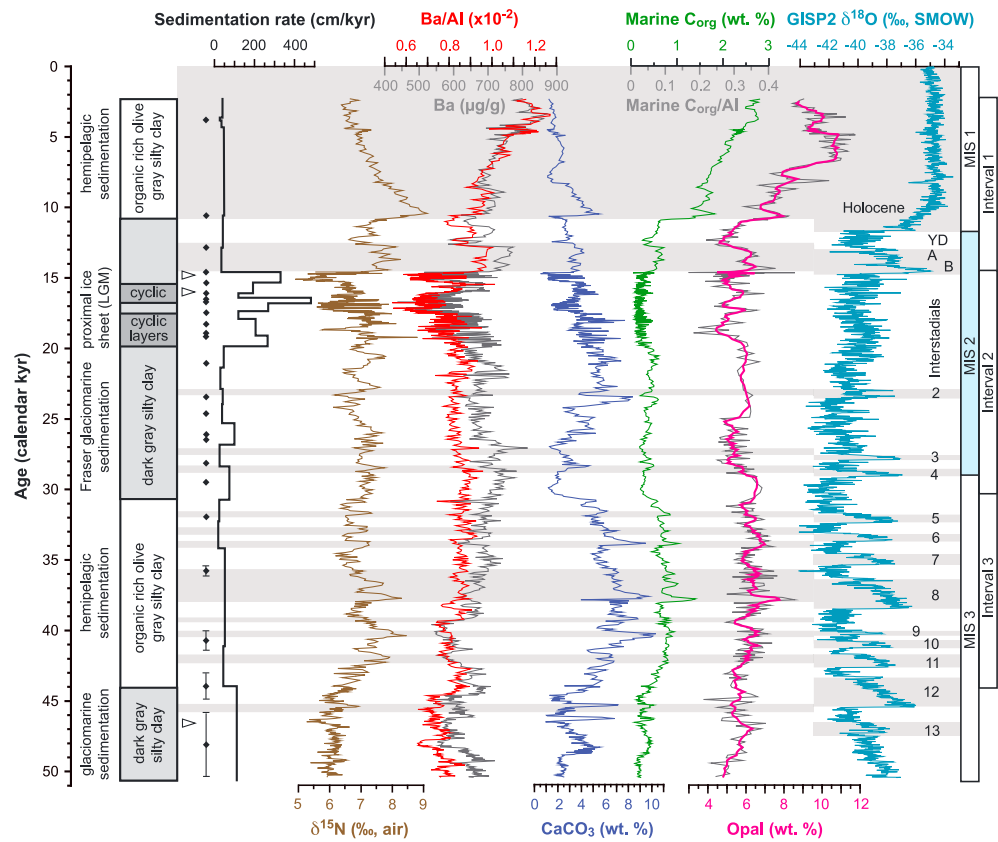
Figure 2. MD02-2496 stratigraphy, radiocarbon datums, nitrogen isotope ratios (δ^{15}N), and productivity proxies (Ba, CaCO$_3$, marine C$_{org}$, and opal). Depositional events from *Hendy and Cosma* [2008]. Stratigraphy determined from *Beaufort et al.* [2002]; white arrowheads denote major intervals of ice-rafted debris. Radiocarbon datums (calendar years, black diamonds) and sedimentation rate from *Cosma et al.* [2008]. Vertical bars on datums are error ranges; datums without bars indicate error ranges spanning the height of the symbol or less. Marine C$_{org}$/Al profile is nearly identical to the C$_{org}$ profile. Bold opal curve is a five-point running average. Greenland Ice Sheet Project (GISP) 2 record and interstadials (gray bands at right) from *Dansgaard et al.* [1993] and *Stuiver and Grootes* [2000]; SMOW: standard mean ocean water. Horizontal gray bands behind MD02-2496 data are warm climate intervals defined by GISP2 interstadials. YD: Younger Dryas, A: Allerød, B: Bølling. LGM: Last glacial maximum. Marine Isotope Stage (MIS) boundaries from *Lisiecki and Raymo* [2005], with glacial MIS shaded blue. Statistical correlations performed for Intervals 1–3; see section 3.4.

warmer climatic intervals (Figure 3). Only U/Al ratios are above the lithogenic background throughout the record. Silver concentrations range from 18 to 708 ng/g, Cd from 0.05 to 1.42 µg/g, Re from 0.2 to 34.6 ng/g, U from 1.5 to 6.8 µg/g, and Mo from 0.4 to ~7 µg/g. Of all the metals, Ag shows the highest fidelity with IS events, with 100–200 ng/g increases from baseline, and has a similar structure with the profiles of sedimentary δ^{15}N and marine C$_{org}$ during Marine Isotope Stage (MIS) 3 (Figure 2), especially during IS 8 with the tri-lobed oscillation. Repeated analysis of single-sample peaks for Cd (~1.1 µg/g increase, beginning of IS 8) and Mo (~5 µg/g increase, IS 9) confirms the high concentrations are real. Discrete increases in U and Mo concentrations (~1 µg/g) occurred when the CIS was proximal to the coring site. All trace elements show large and rapid (spanning ~370 years or 12.5 cm of core depth) increases in concentrations and metal/Al ratios at the beginning of the Holocene, followed by a decrease of similar magnitude until ~9.5 kyr BP, after which the profiles become different from each other to the top of the core.

The major element profiles do not correlate well with IS events (Figure 4). Iron concentrations range from 3.1 to 7.5 wt. %, with values lower than average shale (4.9 wt. %) [*Wedepohl*, 1971] in the hemipelagic sediments. A large Fe enrichment (~2 wt. %) occurs just before IS 12. Manganese concentrations range from 390 to 930 ppm, which are mostly below the average shale concentration (850 ppm) [*Wedepohl*, 1971], with the exception of intervals at ~16–17 and 27 kyr BP.
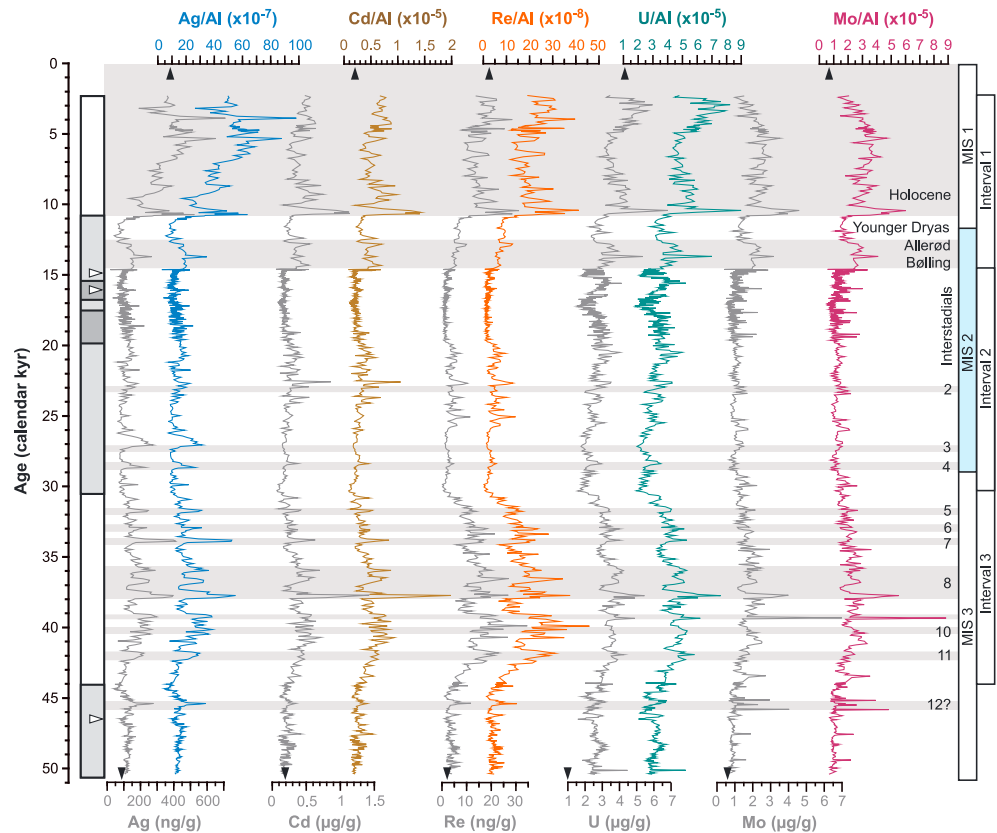
Figure 3. Trace element concentrations (gray curves) and metal/Al ratios (colored curves) from MD02-2496. Typical lithogenous concentrations (black arrowheads) based on oxic surface sediments in the region are 84 ng/g Ag, 0.2 μg/g Cd, 2.1 ng/g Re, 0.6 μg/g Mo [McKay and Pedersen, 2008], and 1 μg/g U [Morford et al., 2001]. Normalizing these background concentrations to the average shale Al concentration [Wedepohl, 1971] yields lithogenous metal/Al ratios of 9.5×10^{-7} Ag, 0.2×10^{-5} Cd, 2.4×10^{-8} Re, 1.1×10^{-5} U, and 0.7×10^{-5} Mo. See Figure 2 for stratigraphy and definitions of abbreviations. Horizontal gray bands are warm intervals in MD02-2496 identified from GISP2 record.

3.4. Statistical Correlations

Because the response of each proxy changes with different depositional environments, statistical comparisons are made for three time intervals (each with $n = 123$ to 150 samples) identified by their distinct climate-related sediment composition (Table 2). Throughout each interval, Al is negatively correlated with opal and marine C_{org}, reflecting a two-component terrigenous and biogenous contribution to the sediments. Interval 1 (~14.7 kyr BP to core top) contains mainly post-glacial hemipelagic sediments and the strongest correlations of any interval. Biogenous components and elements associated with productivity (i.e., marine C_{org}, opal, Ba, and Ag) are strongly and positively correlated to each other ($r = 0.91$, $p < 0.01$ for Ag and opal), while being negatively correlated to elements associated with lithogenous sediments (i.e., Al, Fe, and Mn). Suboxic trace elements (Cd, Re, and U) correlate with the biogenous components, while $\delta^{15}N$ and $CaCO_3$ correlate with the lithogenous elements. Interval 2 (~14.7–30.5 kyr BP) contains Fraser glaciomarine sediments, with weak positive correlations between lithogenous elements (Al, Fe, and Mn), moderate correlations between Cd, U, and $CaCO_3$, and Ba and $\delta^{15}N$, and a strong correlation between marine C_{org} and Re ($r = 0.85$, $p < 0.01$). Cadmium is also correlated to Re and C_{org}, while U is negatively correlated to Mn. Interval 3 (~30.5–44 kyr BP) contains MIS 3 hemipelagic sediments, where the productivity proxies (marine C_{org}, $CaCO_3$, and $\delta^{15}N$, except for Ba and opal) are correlated to the redox elements (Ag, Cd, Re, U, and Mo). Lithogenous elements (Al, Fe, and Mn) are negatively correlated to all of the redox elements and productivity proxies, but are positively correlated with Ba, which behaves like a lithogenous element during this interval. Opal is poorly correlated to all other proxies during Interval 3.
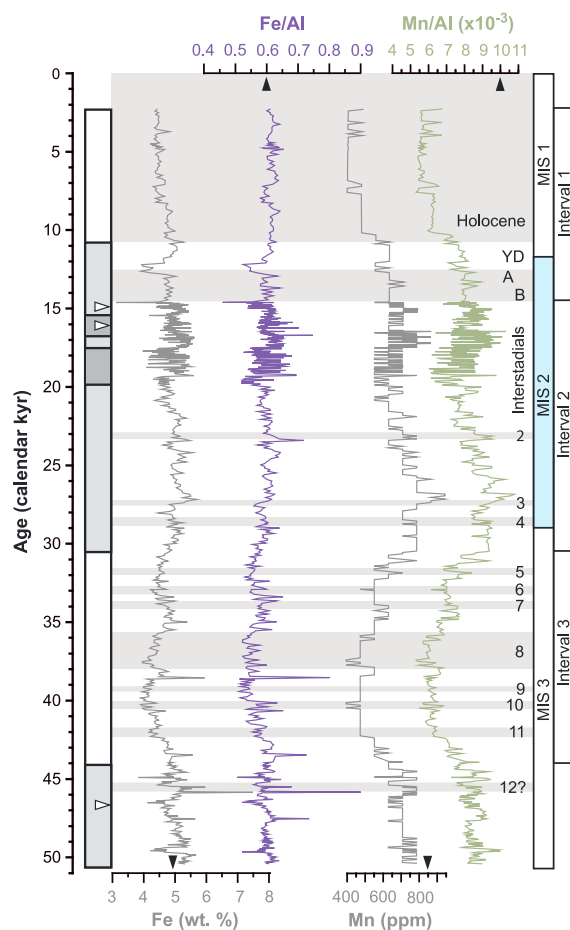
Figure 4. Major element concentrations (gray curves) and metal/Al ratios (colored curves) in MD02-2496. Black arrowheads denote average shale levels for Fe (Fe/Al) of 4.9 wt. % (~0.6), and for Mn (Mn/Al) of 850 ppm (0.01) [*Wedepohl*, 1971]. See Figure 2 for stratigraphy and definitions of abbreviations. Horizontal gray bands are warm intervals in MD02-2496 identified from GISP2 record.

4. Discussion

4.1. Mechanisms of Trace Element Accumulation

Interpretation of paleoenvironmental conditions requires understanding of site-specific processes that control elemental distributions in sediments. The authigenic accumulation of chalcophile and redox-sensitive trace elements in sediments has been extensively reviewed by *Crusius et al*. [1996], *Nameroff et al.* [2002, 2004], *Tribovillard et al.* [2006], *Calvert and Pedersen* [2007], *McKay et al.* [2007], and *McKay and Pedersen* [2008]. Trace elements that are not bound in lithogenous materials (aluminosilicate lattices) accumulate in the sediments depending on their redox state (e.g., Re and U), their speciation (e.g., Mo), or the presence of sulfide (e.g., Ag, Cd, and Mo). Under oxic conditions near the sediment-water interface, trace elements can remain at or below average lithogenous values. As pore water oxygen becomes depleted under suboxic conditions, Re and U diffuse into the sediments along their respective concentration gradients controlled by their removal into the solid phases due to reduction and precipitation/adsorption [*Klinkhammer and Palmer*, 1991; *Colodner et al.*, 1993; *Crusius et al.*, 1996]. Of all the redox-sensitive trace elements whose sedimentary geochemistries are reasonably well understood, Re shows the largest authigenic enrichment with respect to crustal levels, and is not related to Mn or Fe cycling [*Colodner et al.*, 1993; *Crusius et al.*, 1996; *Morford et al.*, 2005]. In addition to reduction, U can be adsorbed onto insoluble Mn-oxyhydroxides and enriched under

oxic conditions [*Brennecka et al.*, 2011], or can be delivered to the sediments with settling organic particles, where U preservation increases in oxygen-poor environments [*Zheng et al.*, 2002]. Insoluble CdS precipitates in the sediments when trace amounts of pore water sulfide are present [*Rosenthal et al.*, 1995]. Silver enrichment as highly insoluble Ag_2S [*Dyrssen and Kremling*, 1990] can occur in both suboxic and anoxic sediments [*Koide et al.*, 1986; *McKay and Pedersen*, 2008]. Molybdenum can be enriched in both oxic and anoxic sediments. In oxic conditions, Mo can be adsorbed onto Fe- and Mn-oxyhydroxides in surface sediments [*Shimmield and Price*, 1986], resulting in simultaneous enrichments of Fe, Mn, and Mo. When the oxyhydroxides are dissolved during burial under suboxic conditions [*Calvert and Pedersen*, 1996], Mo can diffuse out of the sediments alongside Fe and Mn, resulting in low Mo concentrations. In anoxic conditions, Mo is immobilized into the solid phase at specific pH and H_2S conditions [*Helz et al.*, 2011] and accumulates in the sediments in the absence of Fe and Mn enrichment.

Weakly suboxic conditions currently occur within millimeters of the sediment-water interface on the continental slope within the vicinity of MD02-2496. This is supported by Mn/Al and Mo/Al ratios that are below background levels, and by low enrichments of Re, U, and Cd (core JT96-09; Figure 1) [*McKay et al.*, 2005]. Silver is enriched at three times above the lithogenous background in near-surface sediments (core JT09mc) [*McKay and Pedersen*, 2008]. Deeper in the sediment column (~15 cm or ~3.3 kyr BP, core JT09mc) [*McKay et al.*, 2007; *McKay and Pedersen*, 2008], the concentrations of Re, U, and Cd increase up to threefold, Ag remains elevated, but Mo is still

Table 2. Correlation Coefficients for Measured Proxies in MD02-2496 During Three Time Intervals (SAS v. 9.4)

Interval 1. Spearman Correlation Coefficients (n = 123), ~14.7 kyr BP to Core Top[a]

	Al	CaCO3	Opal	δ15N	Mar. Corg	Ag	Cd	Re	U	Mo	Ba	Fe
CaCO3	**0.50**											
Opal	**−0.67**	**−0.47**										
δ15N	**0.54**	**0.61**	**−0.31**									
Mar. Corg	**−0.69**	**−0.54**	**0.83**	**−0.42**								
Ag	**−0.62**	**−0.44**	**0.91**	**−0.27**	**0.82**							
Cd	−0.14	−0.11	**0.31**	0.02	**0.47**	**0.39**						
Re	**−0.39**	**−0.24**	**0.58**	−0.06	**0.73**	**0.58**	**0.61**					
U	**−0.37**	−0.13	**0.52**	−0.04	**0.72**	**0.54**	**0.66**	**0.72**				
Mo	−0.12	0.00	**0.48**	0.28	0.24	0.54	**0.36**	**0.31**	**0.36**			
Ba	**−0.37**	*−0.22*	**0.56**	−0.16	**0.75**	**0.60**	**0.48**	**0.60**	**0.68**	*0.18*		
Fe	**0.75**	**0.52**	**−0.31**	**0.54**	**−0.34**	**−0.29**	0.03	−0.11	−0.02	0.14	−0.04	
Mn	**0.78**	**0.53**	**−0.86**	**0.40**	**−0.86**	**−0.85**	**−0.27**	**−0.58**	**−0.53**	**−0.31**	**−0.57**	**0.46**

Interval 2. Spearman Correlation Coefficients (n = 127), ~14.7–30.5 kyr BP[a]

	Al	CaCO3	Opal	δ15N	Mar. Corg	Ag	Cd	Re	U	Mo	Ba	Fe
CaCO3	**−0.48**											
Opal	−0.05	0.15										
δ15N	−0.05	**0.36**	**0.26**									
Mar. Corg	−0.13	**0.28**	**0.25**	*0.18*								
Ag	−0.02	0.02	*0.19*	0.07	**0.26**							
Cd	**−0.34**	**0.60**	*0.21*	**0.33**	**0.59**	**0.26**						
Re	−0.17	**0.23**	*0.20*	0.00	**0.85**	*0.18*	**0.61**					
U	**−0.23**	**0.66**	0.11	0.15	0.14	−0.16	**0.42**	*0.17*				
Mo	−0.06	−0.02	0.16	0.04	**0.26**	0.24	0.23	**0.28**	0.14			
Ba	0.24	0.17	**0.29**	**0.65**	*0.22*	0.04	**0.29**	0.07	0.14	0.08		
Fe	**0.46**	**−0.47**	−0.09	**−0.32**	−0.05	0.16	**−0.30**	−0.09	**−0.51**	0.07	−0.17	
Mn	**0.31**	**−0.46**	−0.03	0.04	0.12	0.11	−0.16	0.09	**−0.65**	0.04	*0.21*	**0.52**

Interval 3. Pearson Correlation Coefficients (n = 150), ~30.5–44 kyr BP[b]

	Al	CaCO3	Opal	δ15N	Mar. Corg	Ag	Cd	Re	U	Mo	Ba	Fe
CaCO3	**−0.58**											
Opal	−0.02	*0.20*										
δ15N	**−0.67**	**0.55**	**0.22**									
Mar. Corg	**−0.41**	**0.55**	**0.42**	**0.61**								
Ag	**−0.36**	**0.52**	**0.31**	**0.54**	**0.77**							
Cd	**−0.40**	**0.43**	**0.25**	**0.51**	**0.73**	**0.68**						
Re	**−0.48**	**0.47**	0.13	**0.52**	**0.61**	**0.57**	**0.62**					
U	**−0.33**	**0.62**	**0.27**	**0.52**	**0.74**	**0.61**	**0.65**	**0.54**				
Mo	−0.05	**0.21**	*0.20*	0.14	**0.36**	**0.35**	**0.45**	0.16	**0.54**			
Ba	**0.67**	**−0.38**	0.03	**−0.51**	**−0.31**	**−0.25**	**−0.38**	**−0.39**	**−0.27**	−0.07		
Fe	**0.43**	**−0.46**	−0.10	**−0.53**	**−0.42**	**−0.40**	**−0.34**	**−0.43**	**−0.39**	−0.02	**0.33**	
Mn	**0.54**	**−0.61**	−0.12	**−0.40**	**−0.59**	**−0.40**	**−0.41**	**−0.49**	**−0.51**	**−0.21**	**0.35**	**0.36**

[a]Spearman correlation for non-linear data; italics p < 0.05, bold p < 0.01.
[b]Pearson correlation for linear data; italics p < 0.05, bold p < 0.01.

low and does not become enriched until ~35 cm depth (~8 kyr BP, core JT96-09) [*McKay et al.*, 2005]. This suggests that Re and U continue to diffuse into the suboxic sediments, while minor sulfide formation at the shallower depth is enough to precipitate Cd but not Mo. The constant high Ag concentration suggests that sedimentary redox conditions are not the primary control. Instead, Ag is likely delivered to the seafloor via sinking organic particles [*McKay and Pedersen*, 2008]. This is discussed further in section 4.3.

The MD02-2496 records show that large and rapid fluctuations of all trace elements occurred throughout the last 50 kyr but with no significant time lag. This can be demonstrated using a steady-state diffusion model comparing Re and Mo authigenesis within the sediment column. Fick's first law for downward diffusion flux, $J = (\Phi/F)D_b(\partial C/\partial z)$, is used, assuming in situ diffusion coefficients (D_b) of 6×10^{-6} cm^2/s for the perrhenate ion and 7×10^{-6} cm^2/s for the molybdate ion [*Li and Gregory*, 1974], a porosity (F) of 0.8 that is typical for Vancouver Island margin sediments [*McKay et al.*, 2007], and a formation factor (F) of 1.3 that is typical for silty clays [*Manheim*, 1970]. The concentrations (C) of dissolved Re and Mo in the bottom
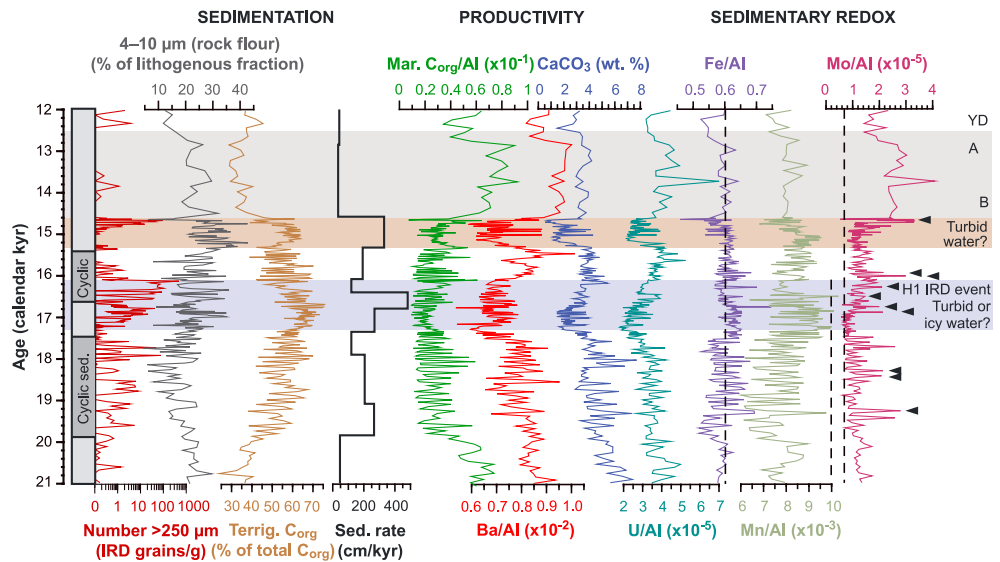
Figure 5. Magnification of MD02-2496 sedimentation, productivity, and sedimentary redox records during a portion of Fraser glaciation. Ice sheet proximity to the coring site occurs during cyclic sedimentation. Grain size data from *Cosma and Hendy* [2008]; IRD: ice-rafted debris. Terrigenous C_{org} fraction from *Chang et al.* [2008]. Vertical dashed lines are metal/Al lithogenous background levels; see Figures 3 and 4 for values and references. Black arrowheads point to possible oxyhydroxide presence, as shown by coincident increases in Mo/Al, Fe/Al, and/or Mn/Al ratios. YD: Younger Dryas, A: Allerød, B: Bølling, H1: Heinrich Event 1. See section 4.4 for explanation of turbid water events.

waters are ~40 pmol/kg [*Anbar et al.*, 1992] and ~100 nmol/kg [*Sohrin et al.*, 1987], respectively, and *z* is the depth below the sediment-water interface where Re and Mo become fixed in the sediments and where pore water Re and Mo are assumed to reduce to zero. At $z = 1$ cm, the estimated flux (J) for Re is ~890 ng/cm^2/kyr. With a sedimentation rate of 46 cm/kyr for the Holocene (Figure 2), and a dry bulk density of 0.5 g/cm^3 [*McKay et al.*, 2007], the estimated sediment mass accumulation rate (MAR) is 23 g/cm^2/kyr. The ratio of J/MAR represents how much Re can be added to the sediments, and at a depth of 1 cm is equal to ~39 ng/g. This is on the same order of magnitude as enrichments seen throughout MD02-2496, signifying that Re is fixed into the sediments at a relatively shallow depth. However, a depth of 1 cm yields a J/MAR ratio for Mo that is an order of magnitude too high (58 μg/g) for what is observed (Figure 3). Instead, $z = 10$ cm yields a J/MAR for Mo of 5.8 μg/g, which is similar to enrichments throughout MD02-2496. These rough calculations illustrate that a difference of 9 cm depth between Re and Mo enrichments yields less than a 200 year lag, which is barely resolvable given our sampling intervals and errors in the age model. The reduction in the enrichment time lag between MD02-2496 and the cores described by *McKay et al.* [2005, 2007] is probably due to better age model controls and a more compacted sediment column in MD02-2496.

4.2. Sedimentary Redox Controls on Trace Element Enrichment

Variations in sedimentary redox conditions on the Vancouver Island margin can be interpreted using a combination of elemental behaviors. The Fe and Mn profiles from MD02-2496 show that increases above the lithogenous background occurred mainly during glaciomarine sedimentation, indicating brief intervals of pore water oxygenation and the burial of oxyhydroxides. Discrete increases in Mo/Al coincident with elevated Fe and/or Mn just before IS 12, or during cyclic sedimentation when the CIS was proximal to the coring site during Fraser glaciation, suggest that Mo was associated with oxyhydroxides and that discrete peaks in U were not (Figures 3 and 5). Instead, U concentration peaks could be due to contributions of U-bearing silts and sands derived from granitic bedrock eroded by the proximal ice sheet, or are co-varying with changes in productivity, although our data cannot differentiate between the authigenic and lithogenous sources of enrichment (Figure 5). A high sedimentation rate (up to 462 cm/kyr) and/or low marine productivity during ice sheet proximity likely led to aerobic pore water conditions. Many of the Fe and

Mn peaks during this time represent single samples covering <100 years of deposition, and the high sedimentation rate may have pushed the redox boundary deep enough for the oxyhydroxides to be preserved during these brief intervals.

For the rest of the record when Fe and Mn are below background, pore waters must have been at least suboxic to prevent the accumulation of oxyhydroxides [*Calvert and Pedersen*, 1996]. Where there is only a minor enrichment of Ag, Cd, Re, and U, such as in glaciomarine sediments older than ~44 kyr BP, near-surface pore waters were likely weakly suboxic, with the exception of the brief oxygenated interval just before IS 12. Uranium concentrations in MD02-2496 during glaciomarine sedimentation are moderately enriched above the reported lithogenous background of 1 μg/g [*Morford et al.*, 2001], suggesting more strongly suboxic conditions. However, these authors reported that their measured U values in reference materials were at least 33% lower than certified values. Thus, the background is likely higher than reported, resulting in a lesser U enrichment in MD02-2496. Where Re, U, Ag, and/or Cd are further enriched without Mo enrichment, bottom and pore waters are interpreted as being more strongly reducing, promoting enrichment of trace elements without Mo sequestration due to continued low levels of dissolved sulfide [*Morford and Emerson*, 1999]. Such conditions in MD02-2496 likely occurred in glaciomarine sediments deposited between ~20 and 22.5 kyr BP before the onset of cyclic sedimentation, between 23.5 and 25 kyr BP prior to IS event 2, and during IS event 4 (Figure 3).

In the portions of MD02-2496 where enrichments in Mo and other trace element concentrations correspond with coeval increases in C_{org}, pore water conditions are interpreted to be anoxic [*Algeo and Lyons*, 2006]. Higher concentrations occur mainly in the organic-rich, hemipelagic sediments, so the assumption is that increased export production led to increased consumption of oxygen in the pore waters during organic matter decay, which subsequently led to the anoxic conditions [*Chang et al.*, 2008].

4.3. Productivity Controls on Trace Element Enrichment

The distributions of dissolved trace elements in the water column reflect their associations with biological activity. The vertical profile of dissolved Cd resembles that of the algal nutrient phosphate [*Bruland et al.*, 1978]. The biological usage of Cd by diatoms has been documented in culture experiments and field-based studies [e.g., *Lee et al.*, 1995; *Lane and Morel*, 2000; *Cullen and Sherrell*, 2005], where Cd is incorporated into the cell cytoplasm [*Reinfelder and Fisher*, 1991]. Thus, Cd has been suggested as a proxy for export production [*Delgadillo-Hinojosa et al.*, 2001]. The vertical profile of dissolved Ag is intermediate between that of nutrient-like and scavenged elements [*Masuzawa et al.*, 1989]. Silver shows a strong positive correlation with silicic acid in the Pacific Ocean [*Zhang et al.*, 2001, 2004; *Kramer et al.*, 2011] but is depleted relative to silicic acid in the OMZ, which is suggestive of removal by scavenging in deeper, oxygen-poor waters [*McKay and Pedersen*, 2008]. Culture experiments show that diatoms assimilate more Ag when concentrations of the nutrients nitrate, ammonium, and phosphate increase, but that only a small fraction of the Ag is incorporated into the cytoplasm [*Xu and Wang*, 2004]. While this suggests that a larger fraction of Ag is incorporated into the diatom frustule, there are no observations from either culture experiments or field samples to confirm this. Nevertheless, the strong correlation between Ag and silicic acid has prompted the proposal that diatoms are the likely vector for Ag delivery to the sediments [*Friedl and Pedersen*, 2001; *Hendy and Pedersen*, 2005; *Wagner et al.*, 2013]. The major carrier of Ba to the sediments is marine barite ($BaSO_4$), which is associated with siliceous debris and decaying particulate organic matter in the water column [*Goldberg and Arrhenius*, 1958; *Bishop*, 1988; *Ganeshram et al.*, 2003; *Paytan and Griffith*, 2007]. Positive correlations between C_{org}, Ag and Ba in continental margin surface and near-surface sediments suggest that sinking organic particles scavenge and deliver Ag to the sediments [*McKay and Pedersen*, 2008].

By contrast to Ag and Cd, the behaviors of dissolved Re, U, and Mo are conservative in the water column [*Collier*, 1985; *Anbar et al.*, 1992; *Singh et al.*, 2011]. While Re and U have no known biological uses, Mo is used by bacteria in biogeochemical processes such as N_2 fixation [e.g., *Tuit et al.*, 2004]. Because the available Mo supply is much greater than the biological uptake [*Nameroff et al.*, 2002], the dissolved Mo profile remains conservative. The enrichment of Re, U, and Mo within the sediments can only be indirectly tied to productivity. For example, recent findings suggest that under favorable conditions during biological sulfate reduction, Re will co-precipitate with a nanoscale Fe-Mo-S phase in the water column [*Helz et al.*, 2011; *Helz and Dolor*, 2012]. Because this phase is too small to settle directly to the sediments, it must be scavenged by sinking organic matter [*Helz and Dolor*, 2012].

Productivity appears to be the primary control on sedimentary redox and trace element accumulation in MD02-2496 during hemipelagic sedimentation of Intervals 1 and 3 (Figures 2–4, Table 2), although subtle differences suggest that upwelling operated differently during each interval. In Interval 3, $\delta^{15}N$, trace elements, and productivity proxies other than Ba all co-vary and are positively correlated. The co-variation and moderate correlations between Ag, marine C_{org}, and $\delta^{15}N$ during the interstadial events of MIS 3 (Figures 2 and 3, Table 2) could suggest some sort of link between Ag and nitrate in diatoms, as illustrated by *Xu and Wang* [2004]. If the California Undercurrent transported enriched nitrate from the ETNP [*Kienast et al.*, 2002], and if coastal upwelling brought that nitrate to surface waters during intermittent warm interstadials, diatoms could have taken advantage of the available nutrients under favorable conditions. Opal preservation is affected by a variety of factors, including diatom abundance and species type (shape, surface area, and robustness), herbivorous grazing and fragmentation, dissolution kinetics, and undersaturation of dissolved Si in sedimentary pore waters [*Ragueneau et al.*, 2000, and references therein]. The moderately low opal concentrations during Interval 3 suggest generally lower diatom productivity and poorer opal preservation, resulting in a weak positive correlation with marine C_{org} ($r = 0.42$, $p < 0.01$). That $CaCO_3$ and marine C_{org} are better correlated ($r = 0.55$, $p < 0.01$) suggests that carbonate-producing plankton also contributed to the organic matter flux, but that organic matter remineralization within the sediments was low enough to prevent carbonate dissolution. The moderate marine C_{org} concentrations coinciding with enriched Cd, Re, and U suggest that sedimentary pore waters were mostly suboxic and not strongly driven by changes in oxidant demand, except during brief intervals of anoxia whenever coincident peaks in C_{org} and Mo concentrations occurred (e.g., start of IS 8). The anti-correlation identified in Ba concentrations suggests post-depositional remobilization of the element in suboxic and anoxic sediments [*McManus et al.*, 1994]. As barite has likely suffered dissolution from sulfate reduction, it is not a paleoproductivity indicator in these older sediments [cf. *Ganeshram et al.*, 1999].

Marine productivity or biogenous sedimentation during Interval 1 differs from Interval 3 in that above ~9.5 kyr BP, paleoproductivity proxy profiles diverge for the first time in the MD02-2496 record. This could reflect a combination of factors, including the beginning of prolonged Holocene warmth and sustained productivity compared to intermittently favorable conditions during MIS 3; post-glacial eustatic sea level rise and the establishment of modern circulation patterns, based on sea-level reconstructions from nearby core MD02-2494 (Figure 1a) [*Dallimore et al.*, 2008]; and/or the trapping of terrigenous sediments within glacially carved coastal inlets, which left the margin relatively enriched in biogenous sediments as sea level rose [*Bornhold and Yorath*, 1984]. High opal and marine C_{org} concentrations in the mid to late Holocene suggest that diatom productivity dominated (Figure 2). At the same time, the decline in $CaCO_3$ concentrations reflects carbonate dissolution in the presence of abundant organic matter, and possibly reduced populations of carbonate-producing plankton. The loss of correlative behavior of $\delta^{15}N$ with other productivity and redox proxies likely reflects either the gradual reduction of denitrification in the ETNP itself, and/or the reduced northward advection of enriched nitrate from the ETNP [*Hendy et al.*, 2004; *Hendy and Pedersen*, 2006]. The co-variation and strong, positive correlations between Ag, marine C_{org}, Ba, and opal during the Holocene suggest that Ag is influenced more by the deposition of diatoms and sinking organic particles than by sedimentary redox conditions [*McKay and Pedersen*, 2008]. The highest Ba and marine C_{org} concentrations coincide in the late Holocene possibly due to reduced oxidative sulfate demand or insufficient time for barite dissolution [cf. *McManus et al.*, 1994], despite strongly suboxic conditions as indicated by enriched Cd, Re, and U at the top of the record (Figure 3). Insufficient oxidative sulfate demand could also explain the lack of co-variation between Mo and marine C_{org} concentrations during the mid to late Holocene.

4.4. Glacial Effects on Sedimentary Redox Conditions

The proximity of the CIS to the MD02-2496 coring site presents a unique opportunity to examine the effects of glaciomarine sedimentation on productivity and sedimentary redox. Interval 2 statistics encompassing Fraser glaciation show different correlation patterns in the measured proxies in contrast to the productivity-driven correlations of Intervals 1 and 3 (Table 2). Further to the discussion in section 4.2 about the preservation of Fe- and Mn-oxyhydroxides during brief oxic intervals, Figure 5 shows that two intervals of elevated IRD and rock flour deposition during the LGM and subsequent retreat could have caused significant turbidity in the waters over the Vancouver Island margin. In conjunction, melting ice that deposited the lithogenous components likely lowered sea surface temperatures, as reflected in the local alkenone paleothermometry record from JT06-09

[*Kienast and McKay*, 2001; *McKay et al.*, 2004]. Turbid water and low sea surface temperatures between ~4 and 7°C (M. A. Taylor et al., Deglacial ocean warming and marine margin retreat of the Cordilleran Ice Sheet in the North Pacific Ocean, submitted to *Earth and Planetary Science Letters*, 2014) are not conducive for primary productivity, as light penetration into surface waters decreases and metabolic processes slow. Two corresponding intervals of low marine C_{org} (e.g., diatoms), $CaCO_3$ (e.g., coccolithophores), Ba/Al (organic particles), and U/Al (suboxic conditions) occur at 17.3–16.2 and 15.3–14.7 kyr BP. The older interval coincides with elevated Fe/Al, Mn/Al, and Mo/Al ratios that are representative of oxic conditions. Due to high sedimentation rates during these intervals, we cannot discount that dilution by terrigenous materials, instead of reduced productivity, produced the lower marine C_{org} concentrations. Depleted $\delta^{13}C_{org}$ ratios from MD02-2496 suggest that terrigenous organic matter composed up to 75% of the total C_{org} deposited at this time [*Chang et al.*, 2008]. In addition, $\delta^{15}N$ ratios during ice sheet proximity reflect dilution of the enriched marine nitrate signal by depleted soil and vegetation nitrogen ($\delta^{15}N = 3.2$ and -1.4‰, respectively) [*Chang et al.*, 2013]. Thus, the strong correlation between Re and marine C_{org} ($r = 0.85$, $p < 0.01$) at this time was likely caused by high terrigenous sediment deposition that both diluted the biogenous component and reduced diffusion of Re into the sediments.

In addition to probable low productivity and/or input of terrigenous fractions, the glacial NPIW may have been better ventilated, leading to generally increased bottom and pore water oxygen contents. Modeling studies show that enhanced ventilation at intermediate depths occurred in the North Pacific during North Atlantic Heinrich events [e.g., *Okazaki et al.*, 2010]. The IRD event at ~16–17 kyr BP coincides with Heinrich Event 1 [*Hendy and Cosma*, 2008], when inferred oxyhydroxides were deposited (Figure 5).

4.5. Regional Teleconnections

Previous comparative studies examined proxy data from multiple sites along the southern CCS, such as the southern Baja California peninsula, (cores GC31/PC08 and MD02-2508) [*Dean et al.*, 2006; *Cartapanis et al.*, 2011], Santa Barbara Basin (ODP 893A) [*Ivanochko and Pedersen*, 2004; *Dean et al.*, 2006], and the southern California margin (ODP 1017E and 1019A) [*Ivanochko and Pedersen*, 2004; *Hendy and Pedersen*, 2005; *Dean et al.*, 2006]. With the exception of the Santa Barbara Basin, where Mo and C_{org} concentrations did not co-vary, likely as a result of ventilation effects instead of productivity changes in this silled basin [*Ivanochko and Pedersen*, 2004], the comparisons showed that broad similarities, but also local differences, occurred between each open margin site. The most obvious similarities are trends of enriched $\delta^{15}N$ and increased C_{org} and Mo concentrations that coincided with millennial-scale D-O oscillations during MIS 3, suggesting the transmission of North Atlantic climate to the North Pacific. A variety of mechanisms have been evoked to explain this teleconnection, including changes in the global water vapor inventory [e.g., *Broecker*, 1997], atmospheric circulation [e.g., *Hostetler et al.*, 1999], and thermohaline circulation [e.g., *Alley and Clark*, 1999] that affected large-scale climate and oceanography; and freshening of the North Atlantic that had far-reaching effects on deep-sea nutrients, primary productivity, and the OMZ [e.g., *Schmittner et al.*, 2007].

Likewise, *Chang et al.* [2008] and *Galbraith et al.* [2008] showed that co-variation between late Quaternary $\delta^{15}N$ records not only occurred between sites along the southern CCS, as a result of the northward advection of variably enriched nitrate by the California Undercurrent from the ETNP [*Kienast et al.*, 2002], but went as far north as the Vancouver Island margin, beyond the northern extent of the California Current and into the Gulf of Alaska (ODP 887; Figure 1a) [*Galbraith et al.*, 2008]. Within the limitations of the age models developed for each location, fluctuations in $\delta^{15}N$ from Mexico to Alaska are simultaneous [*Chang et al.*, 2008], suggesting that the California Undercurrent connected all sites along the way. That the undercurrent has a more northerly influence than has been previously reported has been validated by water property survey data showing that the modern undercurrent can travel 11,000 km from its point of origin off southern Baja California to eventually reach the Aleutian Islands [*Thomson and Krassovski*, 2010].

Following on these previous observations of hemispheric and latitudinal teleconnections, we compare Cd/Al as a proxy for both export productivity and sedimentary suboxia, U/Al as a proxy for stronger suboxia, and the classic coupling of Mo/Al for sedimentary anoxia and C_{org} for productvity, between the Vancouver Island, southern California, and Baja California margins where all data were available (Figure 6). It is not surprising to see that productivity, sedimentary redox, and trace element accumulation trends during MIS 1, the YD, B/A, and MIS 3 on the Vancouver Island margin are mostly similar to the southern sites, as dictated by the teleconnective influences of North Atlantic climate and the California Undercurrent. The similarities exist
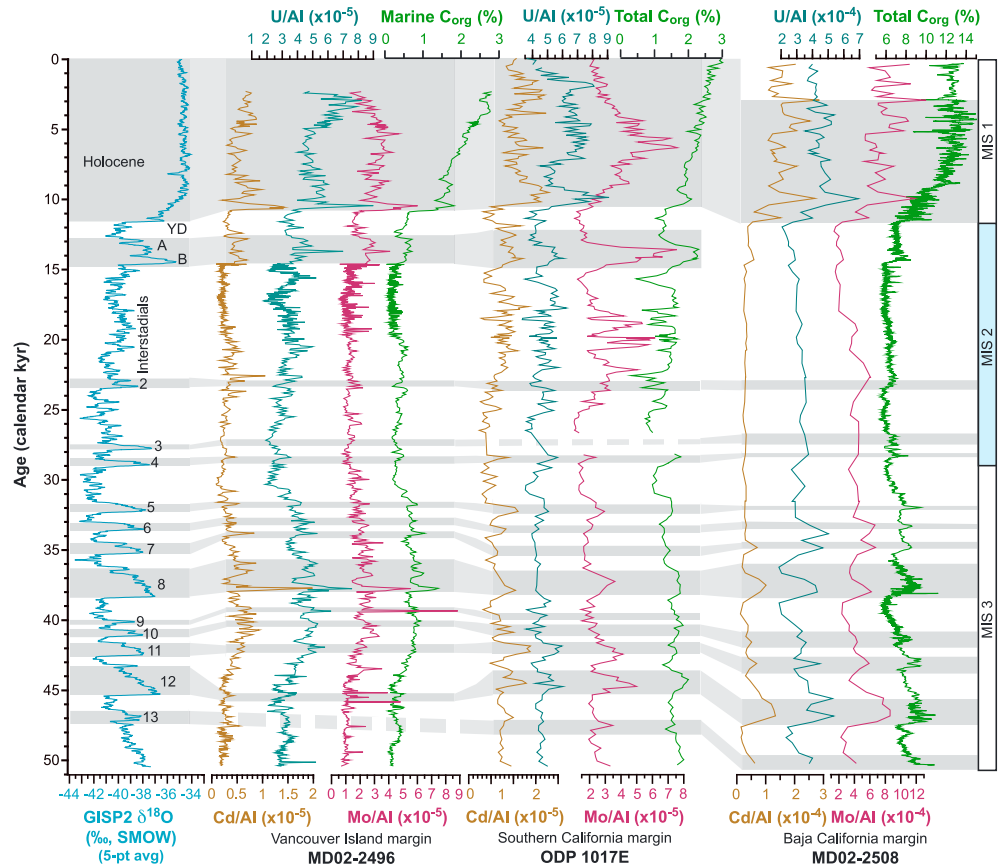
Figure 6. Comparison between GISP2 record, and productivity and sedimentary redox records from sites along the California Current (Figure 1). Abbreviations defined in Figure 2. Southern California margin data from *Hendy et al.* [2004] and *Hendy and Pedersen* [2005]. Baja California margin metal data from *Cartapanis et al.* [2011]; organic carbon data from *Blanchet et al.* [2007], plotted here as a five-point running average. Data for each core are plotted on independently derived time scales. Horizontal gray bars behind MD02-2496 and ODP 1017E data are warm intervals identified from GISP2. Horizontal gray bars behind Baja California data are intervals of laminated sediments [*Cartapanis et al.*, 2011]. Dashed bars represent correlations not identified in the original studies.

regardless if the sediments are laminated (Baja California margin) or not (Vancouver Island and California margins). Laminated sediments are only preserved when bottom water dissolved oxygen contents are <5 μM [*Zheng et al.*, 2000], causing the exclusion of bioturbating macrobenthos in the sediments. Thus, the comparative results illustrate that pore water oxidative demand is more important than bottom water oxygen concentrations and/or fluctuations in the OMZ in controlling the accumulation of trace elements in the sediments during warm climate intervals, and that trace element enrichment can and does occur in the absence of laminated sediments.

Differences in the proxy records at each coring location appear during MIS 2 glaciation. While each location shows a slight increase in C_{org} (productivity) at ~24–25 kyr BP, only MD02-2496 records a distinctive drop in C_{org} between ~20 and 14.7 kyr BP when the CIS reached the continental shelf off Vancouver Island. At ODP 1017E (955 m water depth), moderate Cd/Al ratios and high C_{org} concentrations are suggestive of sustained productivity due to a persistent upwelling cell over the margin [*Hendy et al.*, 2004; *Hendy and Pedersen*, 2005]. Because C_{org} and Mo do not correlate, the high Mo/Al ratios were explained by downslope sediment movement, due to low sea level and a transgressive shoreline on the California coast, leading to Mn-oxyhydroxide deposition in the sediments [*Hendy and Pedersen*, 2005]. Higher oxygen concentrations in pore waters at ODP 1017E between 17 and 14.7 kyr BP are indicated by high I concentrations relative to Br [*Hendy and Pedersen*, 2005; *Hendy*, 2010]. At MD02-2508 (606 m water depth), increases in U/Al and Mo/Al do not co-vary with Cd/Al or C_{org} during MIS 2 [*Cartapanis et al.*, 2011]. These authors suggested that U and Mo enrichments were related more to ventilation changes than to productivity, and that the OMZ became

slightly less oxygenated when ventilated NPIW went below coring depth and occurred deeper in the water column (1000–4000 m) in the glacial ocean [*Matsumoto et al.*, 2002; *Herguera et al.*, 2010].

Contrarily, as explained in section 4.4, the Vancouver Island margin experienced intermittent oxic conditions as a direct result of when the melting CIS led to increased terrigenous sedimentation and reduced productivity. Because MD02-2496 was extracted from a deeper water depth (1243 m) than MD02-2508, a deeper glacial NPIW situated at 1000–4000 m could allow for overall improved oxygenation of bottom and pore waters, making ventilation an additional contributing factor in affecting sedimentary redox on the Vancouver Island margin. Another factor could be a reduced oxidative demand on NPIW during deglaciation. *Crusius et al.* [2004] suggested that apparent reduced ventilation of NPIW during the B/A could be explained by increased productivity near the site of NPIW formation. Here, we suggest that reduced productivity in the turbid water on the marine margin of the CIS during deglaciation (17–14.7 kyr BP) could have reduced the oxidative demand on local NPIW.

5. Summary and Conclusions

High-resolution trace element records from core MD02-2496 on the Vancouver Island margin provide insights into the effects of productivity, glaciation, and ventilation on sedimentary redox conditions over glacial/interglacial time scales. New records of Al, Fe, Mn, Ba, Ag, Cd, Re, and U, together with previously published sedimentology, sedimentary δ^{15}N, $CaCO_3$, marine C_{org}, opal, and Mo data from the same core [*Hendy and Cosma*, 2008; *Chang et al.*, 2008], extend paleoceanographic information to the northernmost extent of the California Current system (CCS).

The trace element records suggest that enrichments resulted from suboxic and anoxic pore water conditions as a response to enhanced primary and export productivity during the warm climate intervals of Marine Isotope Stages (MIS) 1 and 3. Enrichments of Ag were most likely associated with diatoms and sinking organic matter, given the positive correlations of Ag with opal, Ba, and marine C_{org}, furthering the use of Ag as a paleoproductivity indicator. Cadmium is moderately related to marine C_{org}, with Cd enrichment correlated with Re and U enrichments under suboxic conditions. Brief sedimentary anoxic conditions occurred during warm D-O oscillations, as indicated by enrichments of Mo and marine C_{org}. These relationships between trace element enrichment and productivity are similar along the CCS, illustrating geographically large-scale sensitivity of sedimentary redox conditions to variable productivity as a response to climate and oceanographic changes in the North Atlantic and tropical North Pacific.

What distinguishes the Vancouver Island margin from its southern counterparts along the CCS is the direct influence of the Cordilleran Ice Sheet (CIS). During MIS 2, the encroachment of the CIS onto the Vancouver Island continental shelf led to reduced sea surface temperatures, increased terrigenous deposition (rock flour, ice-rafted debris, and terrigenous organic matter) and reduced local productivity (marine C_{org}, opal, and $CaCO_3$). In combination with the likelihood of improved glacial-ocean ventilation, intermittent pore water oxic conditions occurred, resulting in the deposition of oxyhydroxides. Glaciomarine sedimentation does not directly impact paleoceanographic reconstructions elsewhere along the CCS, making the Vancouver Island margin region unique in recording the response of productivity and sedimentary redox conditions to ice sheet sediment delivery.

References

Algeo, T. J., and T. W. Lyons (2006), Mo–total organic carbon covariation in modern anoxic marine environments: Implications for analysis of paleoredox and paleohydrogeographic conditions, *Paleoceanography*, *21*, PA1016, doi:10.1029/2004PA001112.

Allen, S. E., and B. M. Hickey (2010), Dynamics of advection-driven upwelling over a shelf break submarine canyon, *J. Geophys. Res.*, *115*, C08018, doi:10.1029/2009JC005731.

Alley, R. B., and P. U. Clark (1999), The deglaciation of the northern hemisphere, *Annu. Rev. Earth Planet. Sci.*, *27*, 149–182, doi:10.1146/annurev.earth.27.1.149.

Altabet, M. A., and R. François (1994), Sedimentary nitrogen isotopic ratio as a recorder for surface ocean nitrate utilization, *Global Biogeochem. Cycles*, *8*, 103–116, doi:10.1029/93GB03396.

Anbar, A. D., R. A. Creaser, D. A. Papanastassiou, and G. J. Wasserburg (1992), Rhenium in seawater: Confirmation of generally conservative behavior, *Geochim. Cosmochim. Acta*, *56*, 4099–4103, doi:10.1016/0016-7037(92)90021-A.

Andersen, B. C., and H. W. Borns Jr. (1997), *The Ice Age World*, Scandinavian University Press, Oslo, Norway.

Antoine, D., J. M. Andre, and A. Morel (1996), Oceanic primary production. 2. Estimation at global scale from satellite (coastal zone color scanner) chlorophyll, *Global Biogeochem. Cycles*, *10*, 57–69, doi:10.1029/95GB02832.

Beaufort, L., et al. (2002), Les rapports des campagnes à la mer. MD 126 MONA IMAGES VIII Cruise Report, Institute Polaire Fr. Paul-Emile Victor, Plouzaneé, France. [Available at http://www.images-pages.org/cruises/images8/MONA_Cruise_Report.pdf.]

Bishop, J. K. B. (1988), The barite-opal-organic carbon association in oceanic particulate matter, *Nature*, *332*, 341–343, doi:10.1038/332341a0.

Blanchet, C. L., N. Thouveny, L. Vidal, G. Leduc, K. Tachikawa, E. Bard, and L. Beaufort (2007), Terrigenous input response to glacial/interglacial climatic variations over southern Baja California: A rock magnetic approach, *Quat. Sci. Rev.*, *26*, 3118–3133, doi:10.1016/j.quascirev.2007.07.008.

Böning, P., H. -J. Brumsack, M. E. Böttcher, B. Schnetger, C. Kriete, J. Kallmeyer, and S. L. Borchers (2004), Geochemistry of Peruvian near-surface sediments, *Geochim. Cosmochim. Acta*, *68*, 4429–4451, doi:10.1016/j.gca.2004.04.027.

Bornhold, B. D., and C. J. Yorath (1984), Surficial geology of the continental shelf, northwestern Vancouver Island, *Mar. Geol.*, *57*, 89–112, doi:10.1016/0025-3227(84)90196-8.

Brennecka, G. A., L. E. Wasylenki, J. R. Bargar, S. Weyer, and A. D. Anbar (2011), Uranium isotope fractionation during adsorption to Mn-oxyhydroxides, *Environ. Sci. Technol.*, *45*, 1370–1375, doi:10.1021/es103061v.

Broecker, W. S. (1997), Mountain glaciers: Recorders of atmospheric water vapor content?, *Global Biogeochem. Cycles*, *11*, 589–598, doi:10.1029/97GB02267.

Bruland, K. W., G. A. Knauer, and J. H. Martin (1978), Cadmium in the northeast Pacific waters, *Limnol. Oceanogr.*, *23*, 618–625.

Calvert, S. E., and T. F. Pedersen (1996), Sedimentary geochemistry of manganese: Implications for the environment of formation of manganiferous black shales, *Econ. Geol.*, *91*, 36–4, doi:10.2113/gsecongeo.91.1.36.

Calvert, S. E., and T. F. Pedersen (2007), Elemental proxies for palaeoclimatic and palaeoceanographic variability in marine sediments: Interpretation and application, in *Paleoceanography of the Late Cenozoic, Part 1, Methods in Late Cenozoic Paleoceanography*, edited by C. Hillaire-Marcel and A. de Vernal, pp. 567–644, Elsevier, Amsterdam, doi:10.1016/S1572-5480(07)01019-6.

Cartapanis, O., K. Tachikawa, and E. Bard (2011), Northeastern Pacific oxygen minimum zone variability over the past 70 kyr: Impact of biological and oceanic ventilation, *Paleoceanography*, *26*, PA4208, doi:10.1029/2011PA002126.

Chang, A. S., T. F. Pedersen, and I. L. Hendy (2008), Late Quaternary paleoproductivity history on the Vancouver Island Margin, western Canada: A multiproxy geochemical study, *Can. J. Earth Sci.*, *45*, 1283–1297, doi:10.1139/E08-038.

Chang, A. S., M. A. Bertram, T. Ivanachko, S. E. Calvert, A. Dallimore, and R. E. Thomson (2013), Annual record of particle fluxes, geochemistry and diatoms in Effingham Inlet, British Columbia, Canada, and the impact of the 1999 La Niña event, *Mar. Geol.*, *337*, 20–34, doi:10.1016/j.margeo.2013.01.003.

Clague, J. J., and T. S. James (2002), History and isostatic effects of the last ice sheet in southern British Columbia, *Quat. Sci. Rev.*, *21*, 71–87, doi:10.1016/S0277-3791(01)00070-1.

Clague, J. J., J. E. Armstrong, and W. H. Mathews (1980), Advance of the late Wisconsin Cordilleran ice-sheet in southern British Columbia since 22,000 yr BP, *Quat. Res.*, *13*, 322–326, doi:10.1016/0033-5894(80)90060-5.

Collier, R. W. (1985), Molybdenum in the northeast Pacific Ocean, *Limnol. Oceanogr.*, *30*, 1351–1354.

Colodner, D., J. Sachs, G. Ravizza, K. Turekian, J. Edmond, and E. Boyle (1993), The geochemical cycle of rhenium: A reconnaissance, *Earth Planet. Sci. Lett.*, *117*, 205–221, doi:10.1016/0012-821X(93)90127-U.

Cosma, T., and I. L. Hendy (2008), Pleistocene glacimarine sedimentation on the continental slope off Vancouver Island, British Columbia, *Mar. Geol.*, *255*, 45–54, doi:10.1016/j.margeo.2008.07.001.

Cosma, T. N., I. L. Hendy, and A. S. Chang (2008), Chronological constraints on Cordilleran Ice Sheet glaciomarine sedimentation from core MD02-2496 off Vancouver Island (western Canada), *Quat. Sci. Rev.*, *27*, 941–955, doi:10.1016/j.quascirev.2008.01.013.

Crusius, J., S. Calvert, T. Pedersen, and D. Sage (1996), Rhenium and molybdenum in sediments as indicators of oxic, suboxic and sulfidic conditions of deposition, *Earth Planet. Sci. Lett.*, *145*, 65–78, doi:10.1016/S0012-821X(96)00204-X.

Crusius, J., T. F. Pedersen, S. Kienast, L. Keigwin, and L. Labeyrie (2004), Influence of northwest Pacific productivity on North Pacific Intermediate Water oxygen concentrations during the Bølling-Allerød interval (14.7–12.9 ka), *Geology*, *32*, 633–636, doi:10.1130/G20508.1.

Cullen, J. T., and R. M. Sherrell (2005), Effects of dissolved carbon dioxide, zinc, and manganese on the cadmium to phosphorus ratio in natural phytoplankton assemblages, *Limnol. Oceanogr.*, *50*, 1193–1204.

Dallimore, A., R. J. Enkin, R. Pienitz, J. R. Southon, J. Baker, C. A. Wright, T. F. Pedersen, S. E. Calvert, T. Ivanochko, and R. E. Thomson (2008), Postglacial evolution of a Pacific coastal fjord in British Columbia, Canada: Interactions of sea-level change, crustal response, and environmental fluctuations—results from MONA core MD02-2494, *Can. J. Earth Sci.*, *45*, 1345–1362, doi:10.1139/E08-042.

Dansgaard, W., et al. (1993), Evidence for general instability of past climate from a 250-kyr ice-core record, *Nature*, *364*, 218–220, doi:10.1038/364218a0.

Dean, W. E., Y. Zheng, J. D. Ortiz, and A. van Geen (2006), Sediment Cd and Mo accumulation in the oxygen-minimum zone off western Baja California linked to global climate over the past 52 kyr, *Paleoceanography*, *21*, PA4209, doi:10.1029/2005PA001239.

Delgadillo-Hinojosa, F., J. V. Macías-Zamora, J. A. Segovia-Zavala, and S. Torres-Valdés (2001), Cadmium enrichment in the Gulf of California, *Mar. Chem.*, *75*, 109–122, doi:10.1016/S0304-4203(01)00028-7.

Dyrssen, D., and K. Kremling (1990), Increasing hydrogen sulphide concentrations and trace metal behaviour in the anoxic Baltic waters, *Mar. Chem.*, *30*, 193–204, doi:10.1016/0304-4203(90)90070-S.

Friedl, G., and T. F. Pedersen (2001), Silver as a new tracer for diatom production, *EAWAG News*, *52*, 14–15.

Galbraith, E. D., M. Kienast, S. L. Jaccard, T. F. Pedersen, B. G. Brundle, and T. Kiefer (2008), Consistent relationship between global climate and surface nitrate utilization in western subarctic Pacific throughout the last 500 ky, *Paleoceanography*, *23*, PA2212, doi:10.1029/2008PA001518.

Ganeshram, R. S., and T. F. Pedersen (1998), Glacial-interglacial variability in upwelling and bioproductivity off NW Mexico: Implications for Quaternary paleoclimate, *Paleoceanography*, *13*, 634–645, doi:10.1029/98PA02508.

Ganeshram, R. S., S. E. Calvert, T. F. Pedersen, and G. L. Cowie (1999), Factors controlling the burial of organic carbon in laminated and bioturbated sediments off NW Mexico: Implications for hydrocarbon preservation, *Geochim. Cosmochim. Acta*, *63*, 1723–1734, doi:10.1016/S0016-7037(99)0073-3.

Ganeshram, R. S., R. François, J. Commeau, and S. L. Brown-Leger (2003), An experimental investigation of barite formation in seawater, *Geochim. Cosmochim. Acta*, *67*, 2599–2605, doi:10.1016/S0016-7037(03)00164-9.

Garcia, H. E., R. A. Locarnini, T. P. Boyer, and J. I. Antonov (2006), World Ocean Atlas 2005, Volume 3: Dissolved Oxygen, Apparent Oxygen Utilization, and Oxygen Saturation, in *NOAA Atlas NESDIS*, vol. 63, edited by S. Levitus, 342 pp. U.S. Government Printing Office, Washington, D. C.

Goldberg, E. D., and G. O. S. Arrhenius (1958), Chemistry of Pacific pelagic sediments, *Geochim. Cosmochim. Acta*, *13*, 153–212, doi:10.1016/0016-7037(58)90046-2.

Helz, G. R., and M. K. Dolor (2012), What regulates rhenium in euxinic basins?, *Chem. Geol.*, *304–305*, 131–141, doi:10.1016/j.chemgeo.2012.02.011.

Helz, G. R., E. Bura-Nakic, N. Mikac, and I. Ciglenecki (2011), New model for molybdenum behavior in euxinic waters, *Chem. Geol.*, *284*(3–4), 323–332, doi:10.1016/j.chemgeo.2011.03.012.

Hendy, I. L. (2010), Diagenetic behavior of barite in a coastal upwelling setting, *Paleoceanography*, *25*, PA4103, doi:10.1029/2009PA001890.

Hendy, I. L., and T. Cosma (2008), Vulnerability of the Cordilleran Ice Sheet to iceberg calving during late Quaternary rapid climate change events, *Paleoceanography*, *23*, PA2101, doi:10.1029/2008PA001606.

Hendy, I. L., and T. F. Pedersen (2005), Is pore water oxygen content decoupled from productivity on the California Margin? Trace element results from Ocean Drilling Program Hole 1017E, San Lucia Slope, California, *Paleoceanography*, *20*, PA4026, doi:10.1029/2004PA001123.

Hendy, I. L., and T. F. Pedersen (2006), Oxygen minimum zone expansion in the eastern tropical North Pacific during deglaciation, *Geophys. Res. Lett.*, *33*, L20602, doi:10.1029/2006GL025975.

Hendy, I. L., T. F. Pedersen, J. P. Kennett, and R. Tada (2004), Intermittent existence of a southern Californian upwelling cell during submillennial climate change of the last 60 kyr, *Paleoceanography*, *19*, PA3007, doi:10.1029/2003PA000965.

Herguera, J. C., T. Herbert, M. Kashgarian, and C. Charles (2010), Intermediate and deep water mass distribution in the Pacific during the Last Glacial Maximum inferred from oxygen and carbon stable isotopes, *Quat. Sci. Rev.*, *29*(9–10), 1228–1245, doi:10.1016/j.quascirev.2010.02.009.

Herzer, R. H., and B. D. Bornhold (1982), Glaciation and post-glacial history of the continental shelf off southwestern Vancouver Island, British Columbia, *Mar. Geol.*, *48*, 285–319, doi:10.1016/0025-3227(82)90101-3.

Hickey, B. M. (1979), The California Current system—Hypotheses and facts, *Prog. Oceanogr.*, *8*, 191–279, doi:10.1016/0079-6611(79)90002-8.

Hostetler, S. W., P. U. Clark, P. J. Bartlein, A. C. Mix, and N. J. Pisias (1999), Atmospheric transmission of north Atlantic Heinrich events, *J. Geophys. Res.*, *104*(D4), 3947–3952, doi:10.1029/1998JD200067.

Huyer, A., J. A. Barth, P. M. Kosro, R. K. Shearman, and R. L. Smith (1998), Upper-ocean water mass characteristics of the California Current, summer 1993, *Deep Sea Res., Part II*, *45*, 1411–1442, doi:10.1016/S0967-0645(98)80002-7.

Ivanochko, T. S., and T. F. Pedersen (2004), Determining the influences of late Quaternary ventilation and productivity variations on Santa Barbara Basin sedimentary oxygenations: A multi-proxy approach, *Quat. Sci. Rev.*, *23*, 467–480, doi:10.1016/j.quascirev.2003.06.006.

Kienast, S. S., and J. L. McKay (2001), Sea surface temperatures in the subarctic northeast Pacific reflect millennial-scale climate oscillations during the past 16 kyrs, *Geophys. Res. Lett.*, *28*, 1563–1566, doi:10.1029/2000GL012543.

Kienast, S. S., S. E. Calvert, and T. F. Pedersen (2002), Nitrogen isotope and productivity variations along the northeast Pacific margin over the last 120 kyr: Surface and subsurface paleoceanography, *Paleoceanography*, *17*(4), 1055, doi:10.1029/2001PA000650.

Klinkhammer, G. P., and M. R. Palmer (1991), Uranium in the oceans: Where it goes and why, *Geochim. Cosmochim. Acta*, *55*, 1799–1806, doi:10.1016/0016-7037(91)90024-Y.

Koide, M., V. F. Hodge, J. S. Yang, M. Stallard, E. G. Goldberg, J. Calhoun, and K. K. Bertine (1986), Some comparative marine chemistries of rhenium, gold, silver and molybdenum, *Appl. Geochem.*, *1*, 705–714.

Kramer, D., J. T. Cullen, J. R. Christian, W. K. Johnson, and T. F. Pedersen (2011), Silver in the subarctic northeast Pacific Ocean: Explaining the basin scale distribution of silver, *Mar. Chem.*, *123*, 133–142, doi:10.1016/j.marchem.2010.11.002.

Lane, T. W., and F. M. M. Morel (2000), A biological function for cadmium in marine diatoms, *Proc. Natl. Acad. Sci. U.S.A.*, *97*, 4627–4631, doi:10.1073/pnas.090091397.

Lee, J. G., S. B. Roberts, and F. M. M. Morel (1995), Cadmium: A nutrient for the marine diatom *Thalassiosira weissflogii*, *Limnol. Oceanogr.*, *40*, 1056–1063.

Li, Y. -H., and S. Gregory (1974), Diffusion of ions in sea water and in deep-sea sediments, *Geochim. Cosmochim. Acta*, *38*, 703–714, doi:10.1016/0016-7037(74)90145-8.

Lisiecki, L. E., and M. E. Raymo (2005), A Pliocene-Pleistocene stack of 57 globally distributed benthic $d^{18}O$ records, *Paleoceanography*, *20*, PA1003, doi:10.1029/2004PA001071.

Manheim, F. T. (1970), The diffusion of ions in unconsolidated sediments, *Earth Planet. Sci. Lett.*, *9*, 307–309, doi:10.1016/0012-821X(70)90123-8.

Masuzawa, T., S. Noriki, T. Kurosaki, S. Tsunogai, and M. Koyama (1989), Compositional change of settling particles with water depth in the Japan Sea, *Mar. Chem.*, *27*, 61–78, doi:10.1016/0304-4203(89)90028-5.

Matsumoto, K., T. Oba, J. Lynch-Stieglitz, and H. Yamamoto (2002), Interior hydrography and circulation of the glacial Pacific Ocean, *Quat. Sci. Rev.*, *21*(14–15), 1693–1704, doi:10.1016/S0277-3791(01)00142-1.

McKay, J. L. (2003), Palaeoceanography of the northeastern Pacific Ocean off Vancouver Island, Canada, PhD dissertation, University of British Columbia, Vancouver, B. C.

McKay, J. L., and T. F. Pedersen (2008), The accumulation of silver in marine sediment: A link to biogenic Ba and marine productivity, *Global Biogeochem. Cycles*, *22*, GB4010, doi:10.1029/2007GB003136.

McKay, J. L., T. F. Pedersen, and S. S. Kienast (2004), Organic carbon accumulation over the last 16 kyr off Vancouver Island, Canada: Evidence for increased marine productivity during the deglacial, *Quat. Sci. Rev.*, *23*, 261–281, doi:10.1016/j.quascirev.2003.07.004.

McKay, J. L., T. F. Pedersen, and J. Southon (2005), Intensification of the oxygen minimum zone in the Northeast Pacific off Vancouver Island during the last deglaciation: Ventilation and/or export production?, *Paleoceanography*, *20*, PA4002, doi:10.1029/2003PA000979.

McKay, J. L., T. F. Pedersen, and A. Mucci (2007), Sedimentary redox conditions in continental margin sediments (N.E. Pacific) — Influence on the accumulation of redox-sensitive trace metals, *Chem. Geol.*, *238*, 180–196, doi:10.1016/j.chemgeo.2006.11.008.

McManus, J., W. M. Berelson, G. P. Klinkhammer, T. E. Kilgore, and D. E. Hammond (1994), Remobilization of barium in continental margin sediments, *Geochim. Cosmochim. Acta*, *58*, 4899–4907, doi:10.1016/0016-7037(94)90220-8.

Morford, J. L., and S. Emerson (1999), The geochemistry of redox sensitive trace metals in sediments, *Geochim. Cosmochim. Acta*, *63*, 1735–1750, doi:10.1016/S0016-7037(99)00126-X.

Morford, J. L., A. D. Russell, and S. Emerson (2001), Trace metal evidence for changes in the redox environment associate with the transition from terrigenous clay to diatomaceous sediment, Saanich Inlet, BC, *Mar. Geol.*, *174*, 355–369, doi:10.1016/S0025-3227(00)00160-2.

Morford, J. L., S. R. Emerson, E. J. Breckel, and S. H. Kim (2005), Diagenesis of oxyanions (V, U, Re, and Mo) in pore waters and sediments from a continental margin, *Geochim. Cosmochim. Acta*, *69*, 5021–5032, doi:10.1016/j.gca.2005.05.015.

Mortlock, R. A., and P. N. Froelich (1989), A simple method for the rapid determination of biogenic opal in pelagic marine sediments, *Deep Sea Res. Part A*, *36*, 1415–1426, doi:10.1016/0198-0149(89)90092-7.

Nameroff, T. J., L. S. Balistrieri, and J. W. Murray (2002), Suboxic trace metal geochemistry in the Eastern Tropical North Pacific, *Geochim. Cosmochim. Acta*, *66*(7), 1139–1158, doi:10.1016/S0016-7037(01)00843-2.

Nameroff, T. J., S. E. Calvert, and J. W. Murray (2004), Glacial-interglacial variability in the eastern tropical North Pacific oxygen minimum zone recorded by redox-sensitive trace metals, *Paleoceanography*, *19*, PA1010, doi:10.1029/2003PA000912.

Okazaki, Y., A. Timmermann, L. Menviel, N. Harada, A. Abe-Ouchi, M. O. Chikamoto, A. Mouchet, and H. Asahi (2010), Deepwater formation in the North Pacific during the Last Glacial Termination, *Science*, *329*(5988), 200–204, doi:10.1126/science.1190612.

Paytan, A., and E. M. Griffith (2007), Marine barite: Recorder of variations in ocean export productivity, *Deep Sea Res., Part II*, *54*, 687–705, doi:10.1016/j.dsr.2007.01.007.

Peña, M. A., K. L. Denman, S. E. Calvert, R. E. Thomson, and J. R. Forbes (1999), The seasonal cycle in sinking particle fluxes off Vancouver Island, British Columbia, *Deep Sea Res., Part II*, *46*, 2969–2992, doi:10.1016/S0967-0645(99)00090-9.

Pierce, S. D., R. L. Smith, P. M. Kosro, A. F. Barth, and C. D. Wilson (2000), Continuity of the poleward undercurrent along the eastern boundary of the mid-latitude North Pacific, *Deep Sea Res., Part II*, *47*, 811–829, doi:10.1016/S0967-0645(99)00128-9.

Prahl, F. G., J. R. Ertel, M. A. Goni, M. A. Sparrow, and B. Eversmeyer (1994), Terrestrial organic carbon contributions to sediments on the Washington margin, *Geochim. Cosmochim. Acta*, *58*, 3035–3048, doi:10.1016/0016-7037(94)09177-5.

Ragueneau, O., et al. (2000), A review of the Si cycle in the modern ocean: Recent progress and missing gaps in the application of biogenic opal as a paleoproductivity proxy, *Global Planet. Change*, *26*, 317–365, doi:10.1016/S0921-8181(00)00052-7.

Reed, R. K., and D. Halpern (1976), Observations of the California Undercurrent off Washington and Vancouver Island, *Limnol. Oceanogr.*, *21*, 389–398, doi:10.4319/lo.1976.21.3.0389.

Reinfelder, J. R., and N. S. Fisher (1991), The assimilation of elements ingested by marine copepods, *Science*, *251*, 794–796, doi:10.1126/science.251.4995.794.

Rosenthal, Y., P. Lam, E. A. Boyle, and J. Thomson (1995), Authigenic cadmium enrichments in suboxic sediments: Precipitation and post-depositional mobility, *Earth Planet. Sci. Lett.*, *132*, 99–111, doi:10.1016/0012-821X(95)00056-I.

Schmittner, A., E. D. Galbraith, S. W. Hostetler, T. F. Pedersen, and R. Zhang (2007), Large fluctuations of dissolved oxygen in the Indian and Pacific oceans during Dansgaard-Oeschger oscillations caused by variations of North Atlantic Deep Water subduction, *Paleoceanography*, *22*, PA3207, doi:10.1029/2006PA001384.

Shimmield, G. B., and N. B. Price (1986), The behavior of molybdenum and manganese during early sediment diagenesis–offshore Baja California, Mexico, *Mar. Chem.*, *19*, 271–280, doi:10.1016/0304-4203(86)90027-7.

Singh, S. P., S. K. Singh, and R. Bhushan (2011), Behavior of redox sensitive elements (U, Mo and Re) in the water column of the Bay of Bengal, *Mar. Chem.*, *126*, 76–88, doi:10.1016/j.marchem.2011.04.001.

Sohrin, Y., K. Isshiki, and T. Kuwamoto (1987), Tungsten in North Pacific waters, *Mar. Chem.*, *22*, 95–103, doi:10.1016/0304-4203(87)90051-X.

Strickland, J. D. H., and T. R. Parsons (1968), A practical handbook of seawater analysis, Bulletin 167, Fisheries Research Board of Canada, Ottawa.

Stuiver, M., and P. Grootes (2000), GISP2 oxygen isotope ratios, *Quat. Res.*, *53*, 277–284, doi:10.1006/qres.2000.2127.

Sundby, B., P. Martinez, and C. Gobeil (2004), Comparative geochemistry of cadmium, rhenium, uranium and molybdenum in continental margin sediments, *Geochim. Cosmochim. Acta*, *68*, 2485–2493, doi:10.1016/j.gca.2003.08.011.

Takahashi, K. (1998), The Bering and Okhotsk seas: Modern and past paleoceanographic changes and gateway impact, *J. Asian Earth Sci.*, *16*, 49–58, doi:10.1016/S0743-9547(97)00048-2.

Talley, L. D. (1991), An Okhotsk Sea water anomaly: Implications for ventilation in the North Pacific, *Deep Sea Res. Part A*, *38*, S171–S190.

Thomson, R. E., and M. V. Krassovski (2010), Poleward reach of the California Undercurrent extension, *J. Geophys. Res.*, *115*, C09027, doi:10.1029/2010JC006280.

Thomson, R. E., S. F. Mihály, and E. A. Kulikov (2007), Estuarine versus transient flow regimes in Juan de Fuca Strait, *J. Geophys. Res.*, *112*, C09022, doi:10.1029/2006JC003925.

Tribovillard, N., T. J. Algeo, T. Lyons, and A. Riboulleau (2006), Trace metals as paleoredox and palaeoproductivity proxies: An update, *Chem. Geol.*, *232*(1–2), 12–32, doi:10.1016/j.chemgeo.2006.02.012.

Tuit, C., J. Waterbury, and G. Ravizza (2004), Diel variation of molybdenum and iron in marine diazotrophic cyanobacteria, *Limnol. Oceanogr.*, *49*, 978–990.

Van Scoy, K. A., D. B. Olson, and R. A. Fine (1991), Ventilation in the North Pacific intermediate waters: The role of the Alaskan Gyre, *J. Geophys. Res.*, *96*, 16,801–16,810, doi:10.1029/91JC01783.

Wagner, M., I. L. Hendy, J. L. McKay, and T. F. Pedersen (2013), Influence of biological productivity on silver and redox-sensitive trace metal accumulation in Southern Ocean surface sediments, Pacific sector, *Earth Planet. Sci. Lett.*, *380*, 31–40, doi:10.1016/j.epsl.2013.08.020.

Wedepohl, K. H. (1971), Environmental influences on the chemical composition of shales and clays, in *Physics and Chemistry of the Earth*, vol. 8, edited by L. H. Ahrens et al., pp. 307–331, Pergamon, Oxford.

Wyrtki, K. (1962), The oxygen minima in relation to ocean circulation, *Deep Sea Res. Oceanogr. Abstr.*, *9*, 11–23, doi:10.1016/0011-7471(62)90243-7.

Xu, Y., and W.-X. Wang (2004), Silver uptake by a marine diatom and its transfer to the coastal copepod *Acartia spinicauda*, *Environ. Toxicol. Chem.*, *23*, 682–690, doi:10.1897/1551-5028(2004)023<0682:SUBAMD>2.0.CO;2.

Zhang, Y., H. Amakawa, and Y. Nozaki (2001), Oceanic profiles of dissolved silver: precise measurements in the basins of western North Pacific, Sea of Okhotsk, and the Japan Sea, *Mar. Chem.*, *75*, 151–163, doi:10.1016/S0304-4203(01)00035-4.

Zhang, Y., H. Obata, and Y. Nozaki (2004), Silver in the Pacific Ocean and the Bering Sea, *Geochem. J.*, *38*, 623–633.

Zheng, Y., A. van Geen, R. F. Anderson, J. V. Gardner, and W. E. Dean (2000), Intensification of the northeast Pacific oxygen minimum zone during the Bölling-Alleröd warm period, *Paleoceanography*, *15*, 528–536, doi:10.1029/1999PA000473.

Zheng, Y., R. F. Anderson, A. van Geen, and M. Q. Fleischer (2002), Preservation of particulate non-lithogenic uranium in marine sediments, *Geochim. Cosmochim. Acta*, *66*, 3085–3092, doi:10.1016/S0016-7037(01)00632-9.